ELSEVIER

Journal of Food Engineering **36** (1998) 183–200
© 1998 Elsevier Science Limited. All rights reserved
Printed in Great Britain
PII: S0260-8774(98)00026-0 0260-8774/98 $19.00 + 0.00

Simulation of Air Movement in a Dryer by Computational Fluid Dynamics: Application for the Drying of Fruits

E. Mathioulakis, V. T. Karathanos and V. G. Belessiotis

Laboratory of Solar and other Energy Systems, National Centre for Scientific Research 'Demokritos', Agia Paraskevi 15310, Greece

(Received 20 July 1997; accepted 3 February 1998)

ABSTRACT

An industrial batch-type, tray air dryer was constructed for the drying of several fruits. The air movement inside the drying chamber was simulated by computational fluid dynamics (CFD). The pressure profiles and the air velocities in the drying chamber above the product were determined by CFD and a lack of spatial homogeneity of the air velocities above the product was found. Drying tests of several fruits were conducted and the drying result, expressed as weight loss fraction, was determined. There was a variation in the degree of the dryness in several trays and the non-uniformity was traced to in certain areas of the chamber. Comparison of data obtained by the CFD and data obtained from the drying tests showed a strong correlation between the drying rate and the air velocity. © 1998 Elsevier Science Limited. All rights reserved

INTRODUCTION

The drying of agricultural products such as fruits and vegetables is usually performed using the sun. Traditional sun drying takes place under direct sunlight or under transparent plastic films for protection against rain or other environmental factors. Sun drying has the advantages of small installation costs and low drying temperatures while the disadvantages are the long process times, labor cost and the deterioration of the quality due to several factors, such as dust, moisture, insects, etc. A method of increasing importance is the drying of fresh products in large, forced-air circulation dryers at relatively high temperatures to dry the product within a few hours. Such artificial drying has the advantages of controlled drying conditions. It also minimizes the necessity for handling during drying and thus the operating costs are significantly reduced. The risks of several environmental factors,

applied to sun drying, such as rain, dust, insects, problems from stones and other foreign matter, are absent in artificial drying and the dehydrated product is of good quality. Several industrial applications of such food dehydrators working with conventional or renewable energy sources have been reported in recent years (Anonymous, 1994).

On the other hand artificial drying has several disadvantages associated with the cost of equipment, the cost of the consumed energy (thermal and electrical) and the non-uniform drying of the product (Adams & Thompson, 1985). The term 'non-uniformity of drying' means the uneven drying of fruits at various places of a dryer in the case of batch-type equipment. The lack of knowledge of the drying behaviour inside a food dryer may be, at least in part, responsible for the relatively high cost of such a drying installation.

The drying rate is a strong function of air flow or air velocity (Mulet *et al.*, 1987; Karathanos & Belessiotis, 1997). It has been found that the drying rate increases significantly with air flow for the drying of carrots up to an air flow corresponding to an air velocity of *ca* $1{\cdot}5\ \mathrm{m\,s^{-1}}$ (Mulet *et al.*, 1987). Thus it may be of primary importance to know the air flow in the drying chamber, because one may know the areas of adequate or inadequate air velocities, which respectively lead to proper or improper (or slow) drying.

Air movement in air dryers has not been studied extensively. The air flow inside an air drying chamber has been studied by Adams and Thompson (1985), who measured air velocities in a tunnel air dryer. It was found that there was a significant variation of air velocities, which was reduced after the addition of baffles.

In processes which may use air as a reaction or as a heat transfer medium, a simulation of the air movement in the system may be applied, in order to predict the air flow and therefore several transport processes which are connected with the air flow or air velocity.

Computational fluid dynamics (CFD) software may be used to predict air velocities in the drying chamber, because the measurement of air velocities during operation is difficult, since several sensors are needed to be placed at various directions of air flow and locations. The simulation results by CFD may be tested with actual drying experiments and if there is an agreement between predicted and experimental results then the CFD code may be reapplied for other drying conditions to optimize the drying performance of the unit. The CFD may be thus used as a drying optimization tool.

There are no precise references to the literature concerning numerical simulation of air flows in the interior of industrial dryers. There have been significant efforts in the development of algebraic, plug-flow or balance type models (Tsamparlis, 1996), which are based on the assumption of spatial homogeneity of the flow. However, experience has shown that this assumption was not fully verified experimentally. On the contrary, lack of homogeneity often seems to be the main factor of the malfunctioning of dryers.

Numerical simulation, in contrast to the algebraic models, is based on the resolution of Navier–Stokes equations at each point of the field. This kind of model, taking into consideration the exact topography of the plant, is able to describe the spatial and time distributions of velocities, temperatures, pressures and other physically meaningful quantities (Gouvalias *et al.*, 1993). It can also give an explanation for the malfunctioning of dryers and, last but not least, it can lead to the appropriate corrective actions.

DRYER DESCRIPTION

Design of drying chamber

The dryer which was constructed, analysed for its air flow characteristics by CFD and tested was a 5-ton, batch-type, tray air dryer. It was constructed for drying of fruits and vegetables by Vencon-Varsos S.A. (Athens, Greece) to a design developed by NCSR 'Demokritos' and Vencon-Varsos S.A.

The drying chamber of the unit is a chamber having a net length of 6 m, width 2·80 m and net height 2·00 m. The construction is of galvanized iron and the walls and roof are of low thermal conductivity material containing 5 cm insulation. The air, after being heated by a heat exchanger, is distributed by a centrifugal fan through by an air channel located on the upper side of the drying chamber (Fig. 1). The ceiling of the air chamber has a 7% slope in order to direct the air flow from a direction parallel to z-axis towards a direction parallel to the $-y$-axis in the inlet corridor (air channel). It was assumed that this type of design will direct the air uniformly over the drying chamber. The air subsequently turns towards the x-axis and $-x$-axis (symmetrical air flow) and it passes above the product parallel to the trays. The product is placed into trays on racks on both sides of the dryer. The dryer

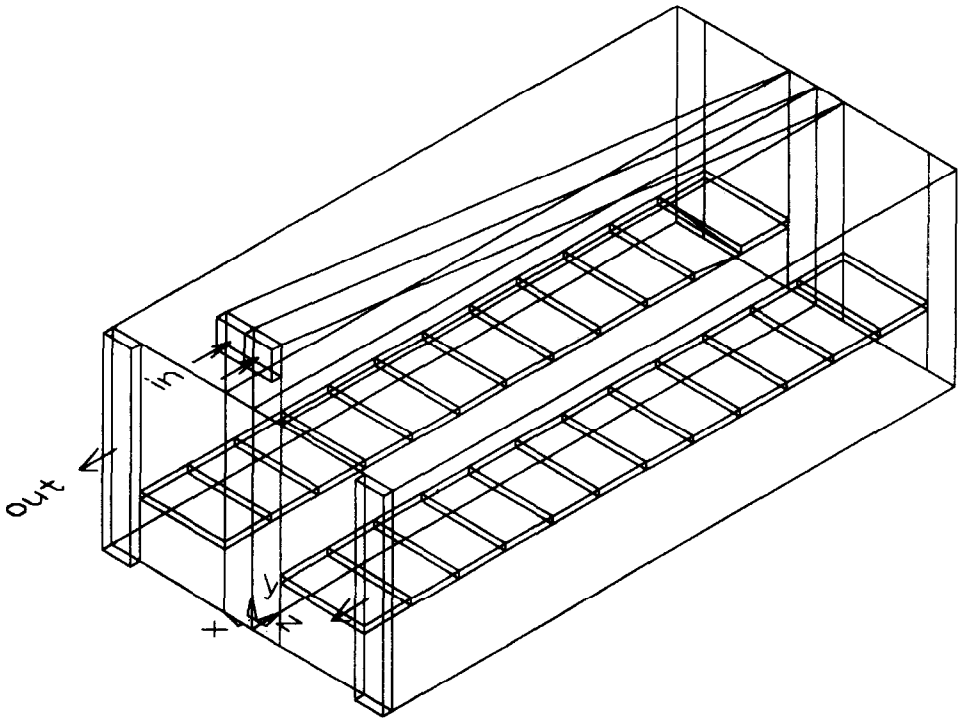

Fig. 1. Drawing of the drying chamber of the tray air dryer. Ìn' and Òut' show the entrance and exit of air from the drying chamber.

is symmetrical around the *yz*-plane. The air is coming out from the product area leaves the drying chamber through two side air channels (corridors) (length 6 m, height 2 m, width 0·3 m) in the $-z$-direction (negative z-direction) and returns to the heating and distribution units.

The dryer was designed as explained in order to allow the air to pass only one tray per pass and may thus be assumed that a uniform drying of all trays would be obtained, due to the similar temperature and relative humidity of the air. Non-uniform drying is a usual limitation of many drying units because of differences in air humidity or temperature as the same air passes from tray to tray (e.g. vertical motion of air in a through-the-trays air movement).

Air heating and distribution

The air was heated using an air/air heat exchanger. The heat was provided by a burner operating with LPG (propane) gas. The air was then forced into the air chamber by a centrifugal fan. Air velocities of *ca* 24 $m\,s^{-1}$ and air flows *ca* 7·6 $m^3\,s^{-1}$ were provided at the entrance of the air to the drying chamber which is located at the upper side of the drying chamber (Fig. 1). The opening was rectangular $0{\cdot}4 \times 0{\cdot}8\ m^2$. After the air passed the product it was returned to the heating section from the two outlet corridors with the aid of two additional smaller identical fans. Part of the air was discharged to keep the moisture of the air inside the chamber constant. The fresh incoming air is preheated by the discharged humid air in two heat exchangers (one per side of the dryer) before being heated to the desired air temperature by the air/air heat exchanger that utilizes the hot gases of the LPG burner. The air at the exit from the drying chamber had an average velocity of *ca* 4·8 $m\,s^{-1}$, almost equal in both of the symmetrical side (outer) corridors.

Tray design and arrangement in the chamber

As said above the product was placed on wooden trays *ca* $0{\cdot}7\ m \times 0{\cdot}5\ m$ ($0{\cdot}35\ m^2$ area), placed on sets of supports on 12 per side of the dryer and *ca* 15 high. The height between trays could be varied to accommodate different products and the number of trays could be varied from 12 to 20 trays per height (288–480 trays total).

Experimental

Several experiments were conducted during the 1996 harvest period. Most of the tests were conducted with figs and currants (one product per cycle) and some with raisins, plums and other products. Most of the product for the tests was of uniform maturity and of good sound quality. No treatment for the fresh product was applied. The product was placed on the trays so as to have an even distribution over the whole area of the tray. In the case of test with currants, on which product the simulation by CFD was based, almost all trays of the dryer (over 98%) were filled with product. Approximately 9 kg (8–10 kg) of fresh product was evenly distributed on each tray at an average height of product 5·5 cm and the drying cycle started as soon as the trays were placed in the chamber.

All trays with currants were weighed accurately at the beginning and the end of the drying cycle using a balance of $\pm 0{\cdot}02$ kg accuracy. The weight reduction after drying was expressed as the ratio of weight lost due to water evaporation per initial net weight of grapes in each tray. The moisture content of the product of several trays was determined at the end of the drying using the drying oven method (vacuum oven for 24 h at 70°C). From the initial moisture content and the optimum final moisture content which should be ca 15% (w.b.) the optimal weight reduction of currants was estimated to be 71% of the initial net weight.

Some air velocities were measured using an anemometer (Ahlborn Almemo Model 8455 (manufactured by AHLBORN, D-83607, Holzkitchen, Germany)). The air flow in the drying chamber was calculated to be *ca* $7{\cdot}6\ \mathrm{m^3\,s^{-1}}$ at both inlet and outlets from the drying chamber. Some velocities above the product were measured by an anemometer and the results agreed remarkably well with the results obtained from the simulation by the CFD code. The air velocity above the product varied from 0·1 to $2{\cdot}5\ \mathrm{m\,s^{-1}}$ with an average air velocity $0{\cdot}8\ \mathrm{m\,s^{-1}}$.

Numerical simulation

The flow geometry and the coordinates system are shown in Fig. 1. The flow field is driven by a pressure gradient which is created outside the drying compartment by the means of a fan. Air flows through a small opening placed in to the top centre of one end the dryer and it is developed to both Z and Y directions in the inlet corridor (buffer). Then the flow passes through the trays in the X direction before leaving the drying compartment through the outlet passages in the $-z$-direction. The main flow pattern, as described already, corresponds to the theoretical circulation scheme of the dryer designer. However, as shown below, the real air course is different. This fact has important consequences for the homogeneity of the drying rate.

Several preliminary tests and temperature measurements have shown that the drying compartment is quasi-isothermal. This is easily explained by considering that the interior of the compartment is characterized by high air velocities and recirculating cells which impose a thermal homogenization of the flow. For this reason and in order to increase the grid density the simulation has been focused on the detailed representation of the three-dimension flow dynamics and the resolution of thermal fields was omitted.

Due to the fact that the main flow evolves in all three directions, the use of a three-dimensional grid is necessary. As a consequence, the dependent variables of the problem are the three velocity components U, V and W in the X, Y and Z directions. Because the flow is forced, the air density and viscosity can be assumed to be constant.

The physical problem can be described by a set of differential equations having the general form:

$$\frac{\partial(\rho\phi)}{\partial t} + \mathrm{div}(\rho V\phi - r\Gamma_{\phi}\nabla(\phi)) = S_{\phi} \tag{1}$$

where ρ is the density in $\mathrm{kg\,m^{-3}}$; ϕ is any conserved property, such as enthalpy, momentum per unit mass, turbulence energy etc, V is the velocity vector in $\mathrm{m\,s^{-1}}$;

Γ_ϕ the exchange coefficient of the entity ϕ, in appropriate units depending on the units of ϕ; and S_ϕ is the source rate of ϕ, in appropriate units depending on the units of ϕ.

Computational grid

For the computation of the above equations, the PHOENICS code was used which is based on the finite volume method, as developed by Patankar and Spalding (1972). The main characteristic of this technique is the immediate discretization of the integral equation of flow into the physical three-dimensional space. For this reason, the computational domain is divided into $NX*NY*NZ$ cells which cover all the drying compartment as well as the inlet and outlet corridors.

The scalar variables (pressure, kinetic energy of turbulence, dissipation rate) are determined at the centre of cells while the three components of velocity are determined on their walls. This approach is known as '*staggered grid arrangement*' (Patankar, 1980).

A crucial factor for the numerical simulation to be realistic is the appropriate definition of the computational grid, which comes as a result of a compromise between the necessity to use a geometry very close to the real one and the necessity to decrease the computational time and achieve a rapid convergence of the numerical process. In this case the existence of a convergent inlet corridor imposed the use of a body fitted coordinates (BFC) computational grid which is able to fit complicated geometry and take the shape of the real flow field (Phoenics, 1991). The trays of fruits were represented as 'blockages', that means solid bodies with zero porosity and friction on their surfaces.

Given the symmetry of the drying chamber the study was made on only one half of the chamber assuming total absence of friction at the interface with the second half (Fig. 1). The simulation assumes 14 rows of trays uniformly distributed over the whole height of the central drying compartment. Finally, after several preliminary trials, a computational grid of $NX = 30$, $NY = 110$ and $NZ = 120$ was implemented representing the best compromise between the available calculation capacity and the efficient discretization of the real geometry. A finer grid would be a great strain on the computational time without significant improvement of the quality of results, while a coarser grid would not allow the realistic representation of the flow, especially in the vicinity of the solids.

Boundary conditions

Setting up of a flow-simulating computation involves specific boundary conditions, in particular at surfaces bounding the domain. In this case the following boundary conditions were implemented:

(1) At the inlet, a fixed-mass-inflow condition was assumed with a velocity of $25\ \mathrm{m\ s^{-1}}$ (measured value) and a turbulence intensity of 4·0% (according to the technical specifications given by the manufacturer of the centrifugal blower).
(2) At the outlet, where mass is allowed to leave the solution domain a no-resistance boundary condition was imposed.

(3) At surfaces bounding the domain, including those bounding trays, a wall shear stress condition was assumed. The viscous sub-layer is bridged by employing a logarithmic-law wall function, to provide near-wall boundary conditions for the mean flow and turbulence transport equations. These formulae therefore connect the wall condition to the dependent variables at the near-wall grid node (Rosten & Worrell, 1988).

The turbulent model

Turbulence is an intrinsic attribute of this type of flow which is characterized by relatively high velocities and the presence of many obstacles. The main objective of the numerical simulation of turbulent flows is to propose a representation of the mean motion. The Navier–Stokes equations of instantaneous motion are averaged to produce the equations of mean motion. The statistical averaging process introduces an unknown turbulent correlation, the so-called *Reynolds stresses* and *fluxes*, in the mean flow equations, which represent the transport of momentum, heat and mass due to turbulence (Spalding, 1982). A *turbulence model* is a set of equations, additional to the averaged Navier–Stokes equations, which may express approximate relationships between otherwise unknown terms and the dependent variables (Tennekes & Lumley, 1972).

The use of different turbulent models might lead to completely different results, especially in a complex geometry configuration. The choice of the appropriate turbulent model must be done after taking into consideration both physical and numerical aspects of the problem. The present configuration is characterized by the presence of many obstacles in the drying room, the development of a jet-type flow in the inlet corridor and the successive variation of main flow direction. Consequently, the use of models which are based on the assumption of isotropic spatial distribution of the turbulence production, as the *constant effective turbulence viscosity* and *standard* k–ε turbulence models, is not recommended (Rodi, 1980). Finally, after several trials, two models proved to be the most suitable:

(1) The so-called *LVEL model* which calculates the effective turbulence viscosity via Spalding's law of the wall. This model is suitable for fluids flowing through spaces cluttered with many solid objects (Phoenics, 1991).
(2) The so-called *Chen–Kim* k–ε *model* which is a variant of the standard k–ε turbulence model performing better than the standard model for flows with streamline curvatures and recirculations (Chen & Kim, 1987).

The two models resulted in very similar results but the Chen–Kim model was finally chosen because of its faster convergence.

RESULTS AND DISCUSSION

Results from the drying of grapes

The product in each tray was relatively uniformly dried and was of an excellent quality, regarding cleanliness, flavour, colour, texture and lack of any foreign matter or other infestation. The only problem with the application of artificial drying in

fruits was the non-uniformity of drying in some areas of the drying chamber, possibly due to the uneven distribution of air flow, since there was no temperature or humidity gradient of inlet air throughout the drying chamber. The variation in air velocities above the product is discussed later. Most of the problems with uneven drying were observed in some trays located in the front part of the drying chamber (Fig. 1) (entrance of air) and some in the middle. The drying of grapes followed a typical drying curve and the drying time was 22 h for $T_{air} = 63°C$.

The data from the analysis of the weight loss in all trays of the dryer showed a variation from 52·7% loss fraction to 74·9% loss for 320 trays with an average weight reduction of 64·8% and a standard deviation of 5·0%. The drying was interrupted at this stage of drying and not at the expected 71% of weight reduction, in order to keep the quality of product in all trays intact. Given that the initial mean moisture content of grapes was *ca* 75%, the average moisture content at the end of drying was 28·5%. For storage stability purposes, some trays of the product, whose drying was incomplete, was additionally dried for limited time (4 h at the same temperature) to complete drying and to result in a product of 15% moisture content (wet basis).

A remarkable similarity of drying was observed between trays located at symmetrical locations in the dryer. The variation of results from tray to tray and the

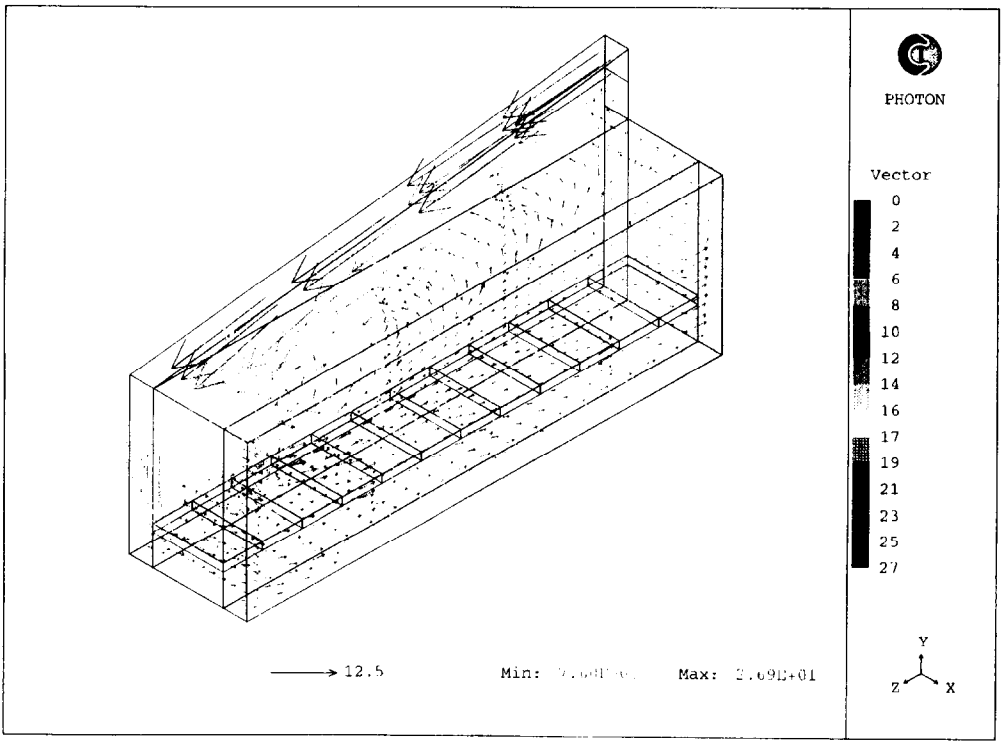

Fig. 2. Velocity vectors in the drying room on planes parallel to the plane (x, z).

inadequacy in drying in several areas necessitated the analysis of air flow in the drying chamber using CFD.

Simulation results by CFD

The simulation was done on a PC Pentium and it took *ca* 10 h computing time, depending on the grid density and the turbulence model. Representative results of the numerical simulation are presented in Figs 2–5. The large grid density (4×10^5 cells) makes it impossible to show the results at every single point of the computational grid. Therefore in Fig. 2 the velocity vectors in the inlet and outer corridor and above the trays are shown by using a less dense grid. The pressure contours are presented in Fig. 3 for two representative planes at plane (y, z) at $x = 0{\cdot}15$ m (lying in the middle of the inlet corridor) and plane (x, z) at $y = 1{\cdot}2$ m (height). The velocity contours of the velocity component W for the above two representative planes at plane (y, z) at $x = 0{\cdot}15$ m and plane (x, z) at $y = 1{\cdot}2$ m are presented in Fig. 4, while the contours for the velocity component U for the same planes are presented in Fig. 5.

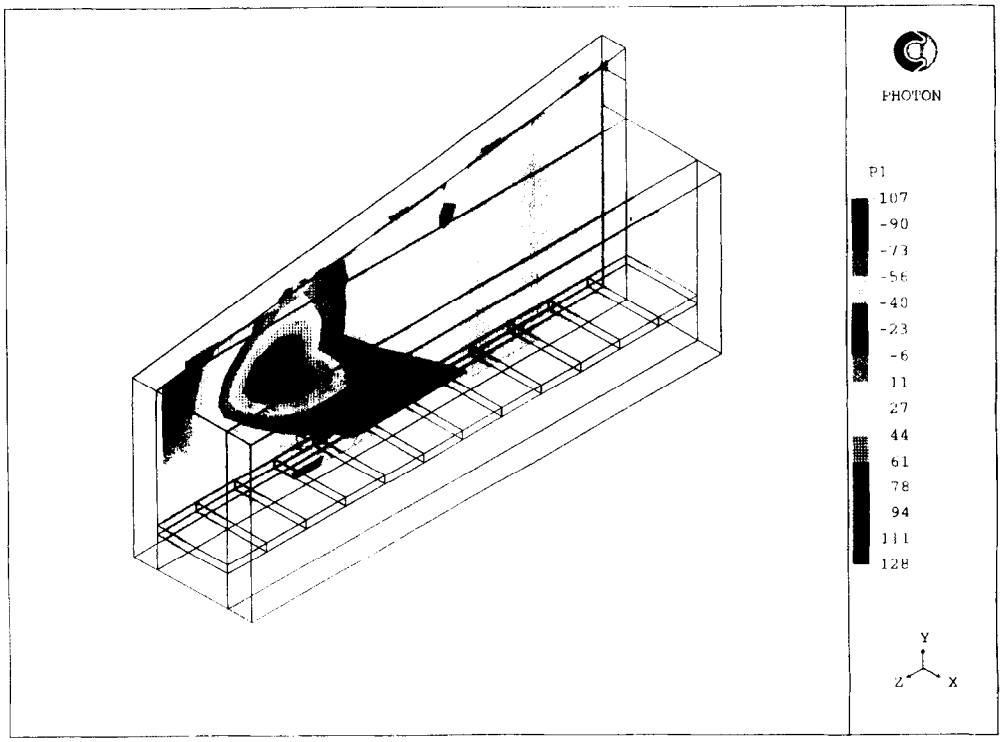

Fig. 3. Pressure contours (in N m^{-2}) on two representatives planes: plane (y, z) at $x = 0{\cdot}15$ m and plane (x, z) at $y = 1{\cdot}2$ m.

The examination of these results, confirms the existence of a serious problem which is related to the lack of spatial homogeneity of the air velocity distribution. This problem is the most important cause of the wide variations in drying rates and moisture content which have been observed in the different parts of the dryer and it constitutes its most serious functional weakness.

More precisely, examination of Figs 2, 3, 4 and 5 shows that:

(1) A large-scale vortex is formed in the inlet corridor, where a jet-type flow is developed associated to a depression region and a strong recirculation. As a consequence, the air circulation is more intense in the rear part of the inlet corridor.
(2) The presence of a low-pressure region at the origin of a horizontal counter-clockwise vortex. The air flow between trays is also characterized by a strong recirculation. Therefore, the air goes directly from the inlet corridor to the outlet corridor only in the last rear part of the drying room ($z > 4$ m). How-

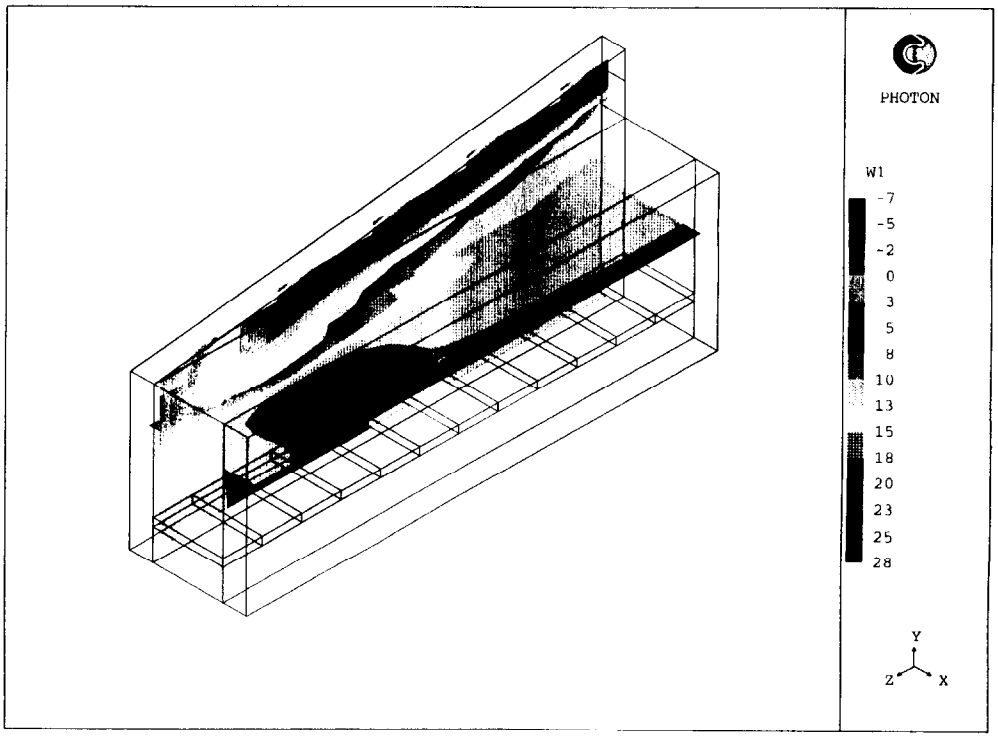

Fig. 4. Contours of velocity component W (in m s^{-1}) on two representatives planes: plane (y, z) at $x = 0{\cdot}15\ m$ and plane (x, z) at $y = 1{\cdot}2$ m.

ever, in the front and central parts of the drying room, the air returns towards the inlet corridor.

(3) The air activity in the space between trays is more important in the rear than in the front and central parts of the drying compartment.

Comparison of drying completeness and air velocity

As stated above there were areas in the drying chamber where the drying was not as advanced as in most other areas of the unit. On the other hand, the CFD simulation showed areas with variable air velocity. These areas are mostly located at the same areas where the lowest drying result was observed. Next the drying result, expressed as percentage of weight reduction (F) due to drying, versus the air velocity above the product, for all trays of the dryer was examined. Some indicative results showing the weight loss fraction (F) as a function of the location of the tray and, on the other hand, the corresponding average air velocities above the product for the same location in the drying chamber are shown in Fig. 6, 7, 8 and 9. In these figures, the average air velocity is taken as the mean value of the total velocities evaluated by

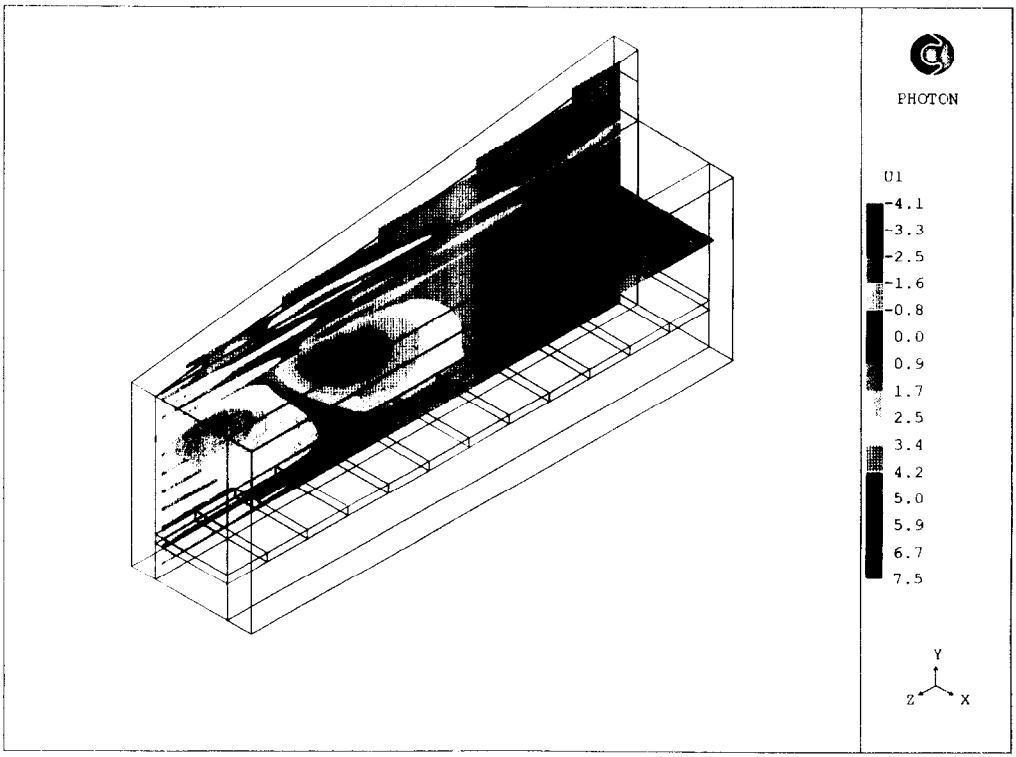

Fig. 5. Contours of velocity component U (in m s^{-1}) on two representatives planes: plane (y, z) at $x = 0{\cdot}15\ m$ and plane (x, z) at $y = 1{\cdot}2$ m.

the model at each grid location above the considered tray. Since the velocity component V was zero (zero velocity on the vertical direction through the product), which was also tested experimentally and numerically to be a true hypothesis, only the velocity components U and W were taken into account.

Figure 6 shows the weight loss fraction (F) in the first column of trays (trays closest to air entrance) for all 14 trays of the column. The other diagram of the same figure depicts the air velocity at the corresponding trays as predicted by the CFD simulation. The drying in this first column was not complete as it did not reach the optimum $F = 0{\cdot}71$ or 71% weight (water) loss according to calculations based on the water content of the material. There are also some areas in this same column where the drying effect was even lower and these are basically the middle trays where the weight loss fraction was lower than $F = 0{\cdot}6$ (incomplete drying). This may be related to the low air velocities above the corresponding trays where the air velocity was $<0{\cdot}5$ m s^{-1}. This is in agreement with the results by Mulet *et al.* (1987) who found that the drying rate may be increased significantly with the increase of air

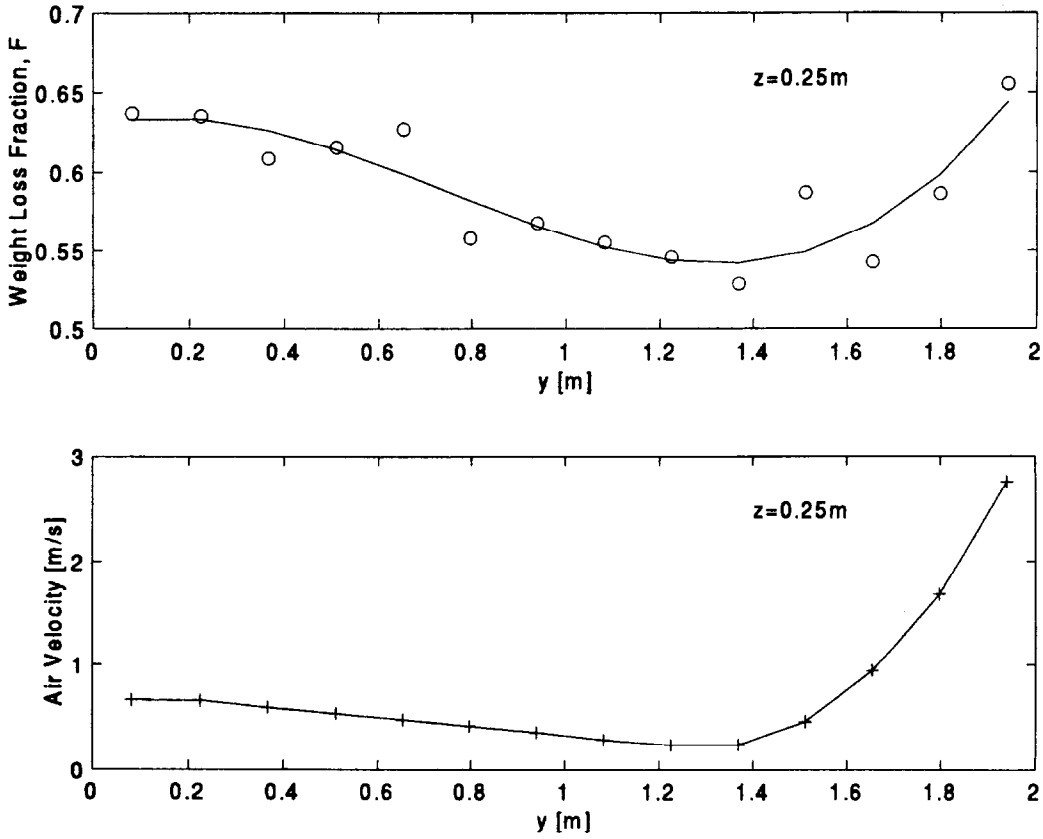

Fig. 6. Weight loss fraction and air velocity above the product as a function of the height of the tray for the column of trays located close to the entrance of air ($z = 0{\cdot}25$ m).

flow (or air velocity) up to an air velocity of *ca* 1·5 m s^{-1}. The relative small drying result in all trays of this column may be due to the fact that the air velocity was in most trays <1 m s^{-1}.

Figure 7 shows F in the third column of trays for all 14 trays of the column. As shown in Fig. 7(b) the air velocity was relatively constant at the lowest trays, *ca* 1 m s^{-1}, and resulted in a constant drying effect (weight loss fraction) equal to *ca* $F = 0{\cdot}61$. At the few upper trays (close to the ceiling of the drying chamber) the air velocity increased, as computed by CFD and resulted in more complete drying which was also found experimentally and is given in Fig. 7(a). Both Fig. 6 and 7 show that there is a relationship between the weight loss fraction F and the air velocity in the y direction (vertical) of the drying chamber at two different positions (z direction) along the dryer (Fig. 1). Similar good relationships may be found for other positions along the dryer (z-axis).

Figurs 8 and 9 show the weight loss fraction F as a function of distance from the entrance of air (along the z direction in Fig. 1). Figure 8 gives the data of the weight

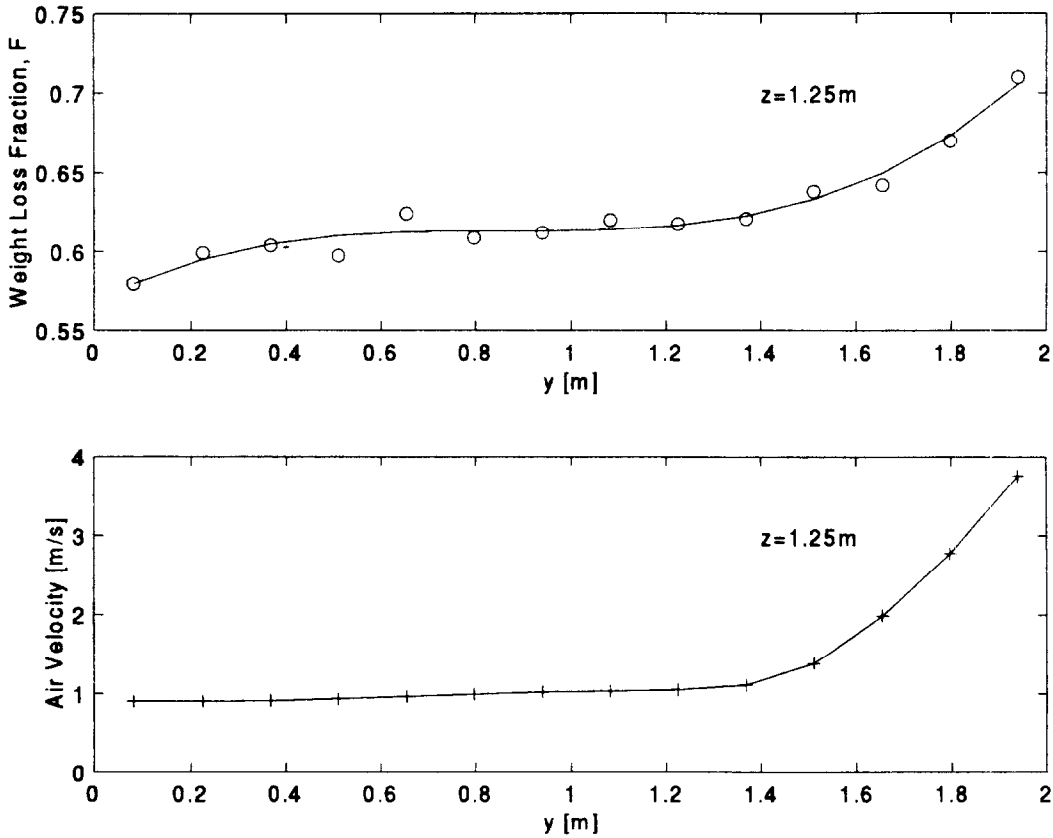

Fig. 7. Weight loss fraction and air velocity above the product as a function of the height of the tray for the third column of trays at $z = 1{\cdot}25$ m.

loss fraction and of the corresponding air velocities along the z-axis of the drying chamber at a height of $y = 0{\cdot}65$ m (approximately one-third of the height or at the 5th tray from the bottom. From this figure it may be seen that there are areas of incomplete drying located basically at the entrance of the air (small z) and another area about in the middle. Both these areas of poor drying effect were predicted through the CFD simulation and resulted in areas of small air velocities, as explained already.

Similar results were obtained from comparison of data for a tray located at a height of $y = 1{\cdot}797$ m (top of column) at various locations along the dryer (z-axis). At these top-located trays the drying was more advanced than in other trays, located at smaller height and the weight loss fraction is close to $F = 0{\cdot}7$ (with the exception of the top trays at the air entrance). From Fig. 9 it may be also seen that there is a direct connection between the drying effect (F) and the air velocity at the corresponding locations. The air velocity in some of these trays was very high and even reached 5 m s^{-1}.

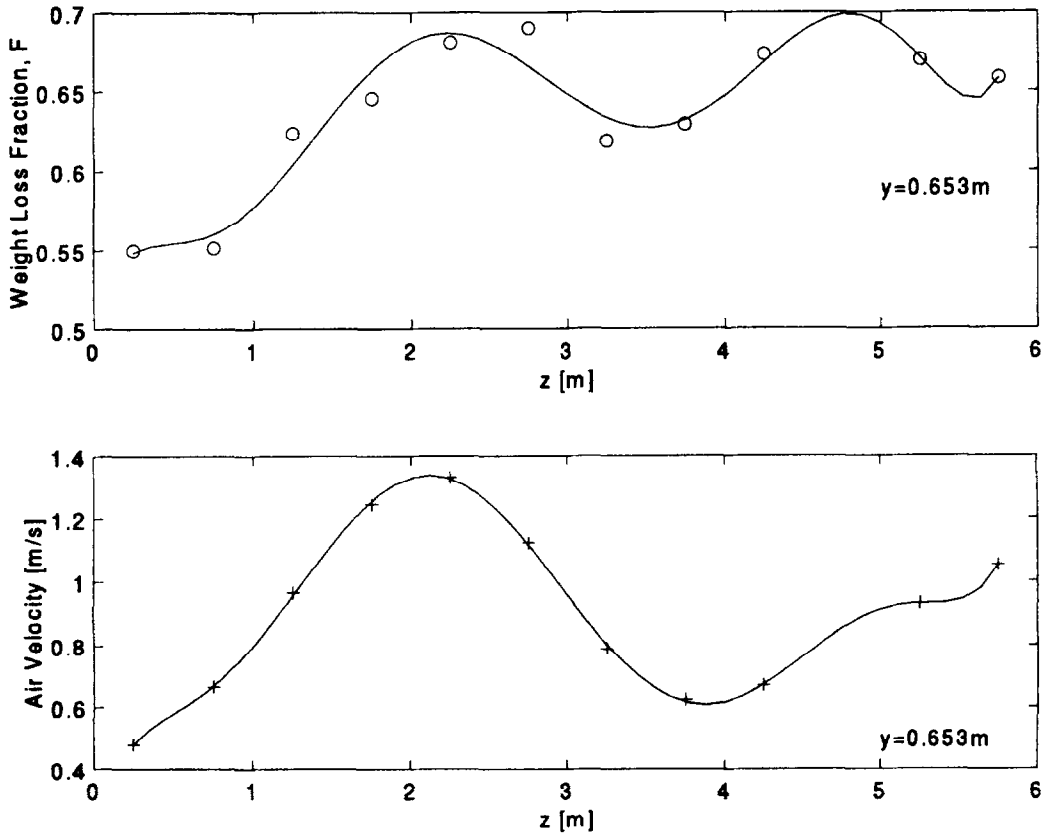

Fig. 8. Weight loss fraction and air velocity above the product as a function of the location of the tray along the dryer (z direction) for a height $y = 0{\cdot}653$ m.

The comparison of weight reduction (F) versus air velocity is reasonable since most of other parameters of air (temperature, air relative humidity) were constant around the drying chamber (before its contact with the product) as measured using appropriate sensors.

All data of F were related to the corresponding air velocity above the tray as shown in Fig. 10. There is a broad variation in the results, due to the fact that the product may vary substantially from tray to tray in terms of maturity and possibly thickness of product bed, although it was placed evenly in the trays. However, there is a rather clear relationship between air velocity and drying effect up to velocities of *ca* 1·2 m s^{-1}. The effect of air velocity on the drying rate is not critical at higher air velocities since the effect of external mass transfer resistance is not a limiting factor for the overall mass transfer process anymore. Similar results have been found by several researchers that there is a critical number of air velocity for

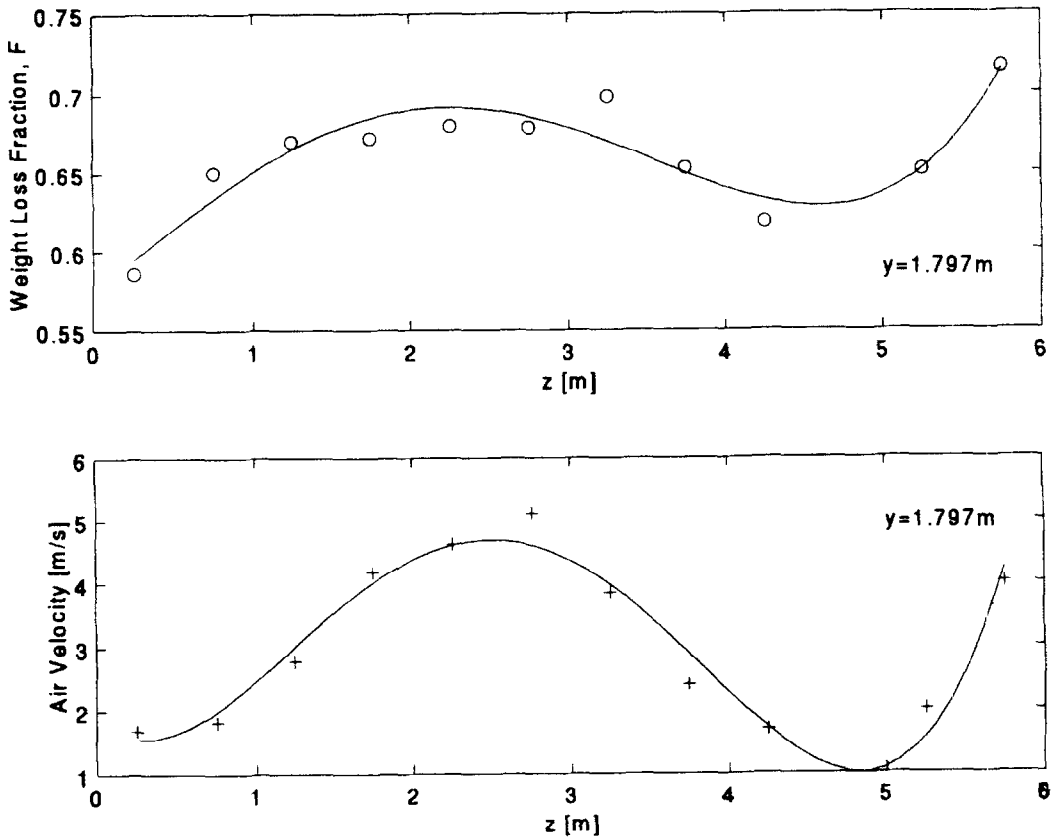

Fig. 9. Weight loss fraction and air velocity above the product as a function of the location of the tray along the dryer (z direction) for a height $y = 1{\cdot}797$ m (close to the top of the chamber).

accelerating the drying process. Mulet *et al.* (1987) determined this value at *ca* $1{\cdot}5\ \mathrm{m\ s^{-1}}$.

Simulation by CFD is an optimization tool in order to avoid unnecessary and costly experiments to improve the design, by applying small improvements in the design of the drying chamber or in the air distribution system. Also using the CFD simulation results, and applying the thin film equation for drying (Morey & Li, 1984; Tulasidas *et al.*, 1993) using the drying constant of the product (Marinos-Kouris & Maroulis, 1995) the time needed for some extra drying for some trays may be predicted, where there is some difficulty to achieving uniform drying. In practice this may be solved by putting product of relatively low moisture in the areas of low air velocities.

The correlation of results concerning the drying factor on one hand and the numerical simulation on the other, shows that CFD could be a reliable tool for the analysis of flow fields developed inside the drying chamber. Therefore, the numerical simulation can be an interesting solution for both the examination of uniformity

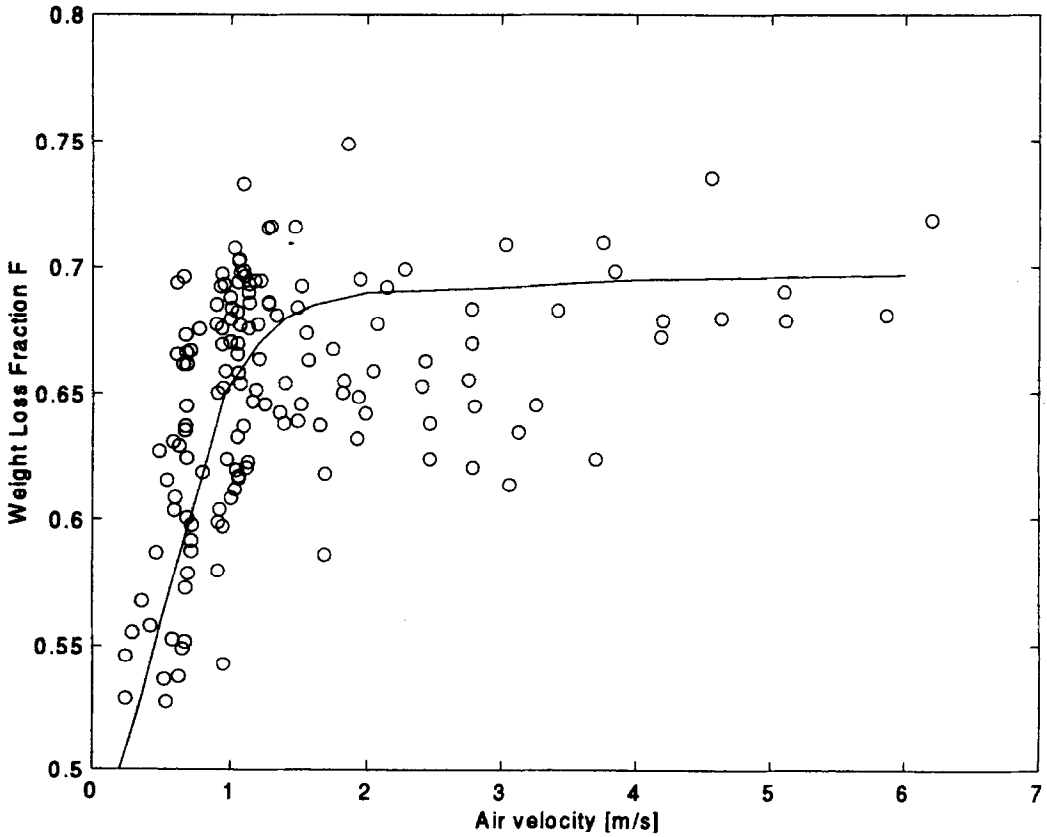

Fig. 10. Correlation of weight loss fraction and air velocity above the product for all the trays of the dryer.

of air flow inside the dryer and the examination of the necessary corrective actions. This is important in the case of industrial dryers, where CFD appears to be a very interesting optimization tool in order to avoid costly and time consuming experimental (trial and error) investigations.

CONCLUSIONS

The data of final moisture content show that the products may not be dried uniformly in this drying chamber, even starting from product of similar maturity. This was related to the air velocity data as found by the simulation for air velocity using CFD. A remarkable correlation between drying completeness and air velocity was found. The data showed that an air velocity $> 1{\cdot}2\ \mathrm{m\ s^{-1}}$ did not result in significant increase in the drying rate.

The CFD data showed that there are two areas of low air velocity, one close to the entrance of the air and the other somewhere in the middle of the drying chamber. The air velocities were related very well to the pressures inside the drying chamber.

Simulation by CFD proved to be a reliable optimization tool in order to avoid unnecessary and costly experiments, to improve the design and to predict the drying time if connected to the thin-film equation.

ACKNOWLEDGEMENTS

This work was partially supported by the Greek Government (Program PENED, Contract No. 1380/96 and partially by the European Union and Greek Government funding (program THERMIE, Project No IN/00196/94/HE). The authors want to thank the Agricultural Cooperative of Kimi, Greece for their contribution in this research.

REFERENCES

Adams, R. L. & Thompson, J. F. (1985). Improving drying uniformity in concurrent flow tunnel dehydrators. *Transactions of ASAE*, **28**(3), 890–892.

Anonymous, (1994). Uses desert's geothermal energy to dehydrate garlic and onion. *Food Technology*, **48**(11), 174

Chen, Y. S. & Kim, S. W. (1987). Computation of turbulence flows using an extended k–ε turbulence closure model, NASA CR-179204. NASA.

Gouvalias, G., Markatos, N. C., Panagopoulos, J., Tierney, M. J., Huberson, S. & Zhong, G. (1993). Advanced flow modeling for industrial applications—CFD models of adsorbers. In *Energy Efficiency in Process Technology*, ed. Pilavachi, P. A. Elsevier Applied Science, London, pp. 374–387.

Karathanos, V. T. & Belessiotis, V. G. (1997). Sun and artificial air drying kinetics of some agricultural products. *Journal of Food Engineering*, **31**(1), 35–46.

Marinos-Kouris, D. & Maroulis, Z. B. (1995). Transport properties in the drying of solids. In *Handbook of Industrial Drying*, ed. Mujumdar, A. S., Vol. 1, 2nd ed. Marcel Dekker, New York, pp. 113–159.

Morey, R. V. & Li, H. (1984). Thin-layer equation effects on deep bed drying prediction. *Transactions of ASAE*, **27**(6), 1312–1316.

Patankar, S. V. (1980). *Numerical Heat Transfer and Fluid Flow*. McGraw–Hill, New York.
Patankar, S. V. & Spalding, D. B. (1972). A calculation procedure for heat, mass and momentum transfer in parabolic flows. *International Journal of Heat and Mass Transfer*, **15**(10), 1787–1806.
Phoenics (1991). *Phoenics Reference Manual*. CHAM/TR200, Phoenics, London.
Rodi, W. (1980). *Turbulence Models and Their Application in Hydraulics: A State of the Art Review*. IAHR, Delft, The Netherlands.
Rosten, H. I. & Worrell, J. K. (1988). Generalized wall functions for turbulent flow. *Phoenics Journal*, **1**(1), 81
Spalding, D. B. (1982). *Turbulence Models: A Lecture Course*. Imperial College, London.
Tennekes, H. & Lumley, J. L. (1972). *A First Course in Turbulence*, 6th ed. MIT Press, Cambridge, MA.
Tsamparlis, M. (1996). Modeling and optimization of a tunnel grape dryer. *Drying Technology*, **14**(7), 1695–1718.
Tulasidas, T. N., Raghavan, G. S. V. & Norris, E. R. (1993). Microwave and convective drying of grapes. *Transactions of ASAE*, **36**(6), 1861–1865.
Mulet, A., Berna, A., Borras, M. & Pinaga, F. (1987). Effect of air flow rate on carrot drying. *Drying Technology*, **5**(2), 245–258.